Paper ID 10974 Session 2022
B2 / Overhead lines
PS1 / Challenges & new solutions in design and construction of new OHL

Design of overhead lines in a changing climate

Emilie C. IVERSEN*
Kjeller Vindteknikk, part of Norconsult
emilie.claussen.iversen@norconsult.com
Norway

Bjørn Egil NYGAARD
Kjeller Vindteknikk, part of Norconsult
bjorn.egil.nygaard@norconsult.com
Norway

Øivind HODNEBROG
CICERO
oivind.hodnebrog@cicero.oslo.no
Norway

Maria SAND
CICERO
maria.sand@cicero.oslo.no
Norway

Kristian INGVALDSEN
CICERO
Norway
kristian.ingvaldsen@norconsult.com

Øyvind WEGAARD
Statnett
Norway
oyvind.welgaard@statnett.no

SUMMARY

Overhead lines (OHLs) are typically designed according to the current or historic climate, based on national codes derived from historic observations or model simulations. With global warming, the frequency and severity of extreme weather events as well as the mean state of the atmosphere will change, affecting the basis for design parameters. Quantitative information about the effects of climate change on these design parameters is therefore of great interest to utilities and other power grid companies responsible for OHL design.

The objective of this work is to quantify changes in design ice loads over all of Norway with the associated uncertainty. This is achieved by creating high-resolution model datasets for future climate, applying dynamical downscaling of global climate models, using a regional model with a limited domain. Two different global climate models with a relatively large spread in climate sensitivity are chosen based on their skill in reproducing the historic climate over Northern Europe. Three different climate change scenarios are also chosen, resulting in the total of six model simulations for the future climate. This results in a span for future ice load estimates, where the spread can be used as a basis for estimation of uncertainty.

The downscaled climate data generally shows an increase in temperature everywhere, except for a relatively small cooling over the North Sea with CESM2 data for the less extreme scenarios. This, and a general increase in warming from west to east is due to the North Atlantic Warming hole (deficit in warming over North Atlantic), which is more prominent in CESM2. The signal in precipitation is less clear, and there are large differences between the two models. For the most extreme scenario where

the signals are most prominent, the downscaling of CESM2 shows precipitation decrease over most of Norway (except southernmost and eastern) while the downscaling of MPI shows an increase over all of Norway. There is stronger agreement in the cloud water signal, where there is a general increase over elevated terrain and decrease in the low land.

Preliminary results of the wet snow icing calculations indicate that change in annual wet snow load total will follow the pattern of precipitation to a large extent, however for coastal, low altitude areas the increased temperature seems to have the largest impact on the total wet snow loads in terms of a reduction. Given that the signal in precipitation is so different between the models, the signal in wet snow load is also varying. Generally wet snow totals are decreasing for terrain below about 400 m.a.s.l. and increasing above, though not true everywhere with CESM2 data, which shows cooling to the west and drying in the western mountains.

The signal in maximum rime ice loads is also very different between the models, despite the agreement in cloud water. The downscaling of CESM2 projects a general increase and of MPI a general decrease in maximum load. This is probably connected to the stronger warming in MPI, which creates more melting episodes.

Further work includes calculation of return values, for both wet snow and rime ice, and investigate the future change. The results will be compiled as maps of change in OHL design ice loads for different future lead times, including uncertainty estimates.

KEYWORDS

Climate change, atmospheric icing, ice loads, OHL design

1. Introduction

Overhead lines (OHLs) are typically designed according to the current or historic climate, based on values provided in national codes derived from historic observations or model simulations. With global warming, the frequency and severity of extreme weather events as well as the mean state of the climate will change. Considering that OHLs are designed with the expected lifetime of about 70 years, climate change impacts on the design parameters should be considered.

In Norway, loads due to atmospheric icing is one of the main meteorological design parameters for OHLs due to the country's northerly location and its topography, including high elevation mountains and a long and exposed coastline. Norway has experienced some of the world's highest recorded ice loads on overhead power lines with measured values exceeding 300 kg/m [1].

There are two types of atmospheric icing that mainly impact the transmission lines in Norway; in-cloud or rime icing due to supercooled liquid cloud droplets that freeze once in contact with the cable; and wet snow icing, which is caused by heavy precipitation in the form of wet snow or sleet at temperatures just above freezing that sticks to the cable [1]. Rime icing typically occurs on elevated and exposed mountains, and particularly close to the coast where moist air masses are advected over land where temperatures are below freezing in winter. The mountainous regions along the western coastline of Norway are particularly exposed as moist air of the westerly North Atlantic flow is lifted over the topography, creating large amounts of clouds in the mountains. Wet snow icing typically occurs in the lowlands for temperatures just above freezing during winter storm events.

In Norway, IPCC projections generally show rising temperatures and more humidity and precipitation in winter [2]. It is though difficult to project future ice loads based on available global- or coarse-scale climate projections, as the loads depend on meteorological variables in combination, and due to the high geographic dependence. For areas experiencing wet snow icing, projections of warming could imply that more winter precipitation will fall as rain. Though, for the same areas, projections of more intense precipitation might indicate larger maximum wet snow loads if temperature stays close to 0°C during extreme events. Cloud water and rime ice is highly dependent on topography and distance to the coast. Projections of more available moisture in the air might indicate larger ice loads and/or more frequent icing. At high altitude mountainous sites extreme ice loads might accumulate over weeks, months or even during a whole winter season if temperature never drops below 0°C. If temperature will exceed 0°C more often in a future climate though, maximum ice loads could decrease. For these reasons, it is clear that climate projections of high spatial resolution as well as detailed treatment of cloud and precipitation physics are needed to meet the objective of assessing the future development of atmospheric ice loads on a regional scale, and furthermore to take this into account in OHL design.

This research is carried out within the Icebox R&D project, led by the Norwegian TSO, Statnett, under the work package concerning mapping of ice loads in historic and future climates. The objective is to quantify changes in design ice loads over Norway with associated uncertainty. The ultimate goal is to create a map of future 50-year return period ice loads, for wet snow and rime ice, to be used by OHL design engineers.

In this paper we will present the methodology used to achieve this objective, as well as some preliminary results. The methodology involves regional downscaling of global climate model data, to obtain the necessary degree of resolution and detail. Two global climate models and three socioeconomic/concentration pathways are used to obtain a spread in climate sensitivity and future realizations, and thereby an estimate of uncertainty. The paper is structured as follows: Section 2 presents the methodology, including selection of climate models, the regional model configuration and downscaling, and a description of the atmospheric icing models. Some preliminary results of the analysis are shown in section 3. Section 4 describes further work.

2. Methodology

Global climate models (GCMs) are the only source available for predictions of future climate. Because they represent the whole globe and are computationally very expensive to run, their resolution is relatively coarse (on the order of 100 km). This causes an unrealistic representation of topography and climate predictions which are averages for large geographic areas. Due to the strong topographic and geographic dependence of atmospheric icing, the GCM data is dynamically downscaled to a finer resolution. It is performed by using a regional atmospheric model with a limited domain, where the GCM data is used as initial and lateral boundary conditions. The regional model used here is WRF (Weather Research and Forecast) [3]. Dynamical downscaling ensures a full representation of physical and dynamical processes, which is important for the relevant meteorological variables here. However dynamical downscaling of GCM data to the required resolution is computationally demanding, and it is not feasible to perform such downscaling for all available GCM data. Therefore, a selection of GCM models and/or climate change scenarios subject to dynamical downscaling have to be made.

Two different GCMs are chosen. Three different climate change scenarios (with emissions resulting from different assumptions of politics, population growth, technological development, etc.) are also chosen, resulting in the total of six model simulations for future climate. Time dependant ice accumulation models are applied with the data, resulting in a span of estimated future ice loads including their geographical distribution. Below is a more detailed description of the methodology.

2.1 Chosen climate models

As atmospheric icing occurs due to moisture, precipitation, temperature and wind, we hypothesize that there is a strong connection between icing and the westerly North Atlantic Storm tracks, at least over the southern half of Norway. The storm tracks are to a large extent controlled by the North Atlantic Oscillation (NAO), which is the leading mode of atmospheric variability in the North Atlantic sector [4]. The NAO index is a measure of the relative strengths of the Icelandic low and Azores high pressure systems. During a positive NAO, low pressure systems typically hit Norway's south-west coast, causing plentiful precipitation and moisture, and relatively mild temperatures. During a negative NAO, storm tracks are typically positioned south of Norway, leaving the country north of the polar front, implying dry and cold weather.

We therefore want to choose GCMs which represent the NAO relatively well and have performed a correlation analysis between available CMIP5 and CMIP6 [5] GCMs and reanalysis data (not shown here). The models AWI-CM-1-1-MR and MPI-ESM1-2-HR (CMIP6) stand out with the highest correlation coefficients, but other models also perform well and reproduce the spatial NAO pattern (e.g CESM2).

We also want to choose GCMs which give a span in climate sensitivity. Climate sensitivity is the global mean surface temperature response to a doubling of atmospheric CO2 concentrations since pre-industrial times. Since impacts of climate change (e.g., on atmospheric icing) are largely determined by how much the Earth warms for a given increase in greenhouse gases, it would be beneficial to choose GCMs that span a range of climate sensitivities.

To obtain an even larger span in future warming, three future realizations, based on a combination of Shared Socioeconomic Pathways (SSPs) and the Representative Concentration Pathways (RCPs), are downscaled with WRF, namely SSP1-2.6, SSP2-4.5 and SSP3-7.0 [6].

Based on the above criteria, as well as suitability for downscaling with WRF, the two GCMs chosen are CESM2 [7] and MPI-ESM1-2-HR [8]. The two models also compare relatively well against ERA5 reanalysis of Arctic surface temperature during 1979-2014 [9]. Their effective climate sensitivity is 5.15 K and 2.98 K for CESM2 and MPI-ESM1-2-HR respectively [10] and this difference is reflected in future projections of global mean surface temperature (Fig. 1, top), where CESM2 projects stronger global warming than the CMIP6 ensemble mean and MPI-ESM1-2-HR projects weaker warming.

However, over our region of interest, the temperature evolution in MPI-ESM1-2-HR is closer to the ensemble mean while the CESM2 is among the models with weakest warming (Fig. 1, bottom). The reason for the weak warming in CESM2 is a phenomenon called the North Atlantic warming hole, which is linked to a slowdown of the Atlantic meridional overturning circulation [11]. The warming hole in CESM2 is strong [12] and one of the strongest among the CMIP6 models.

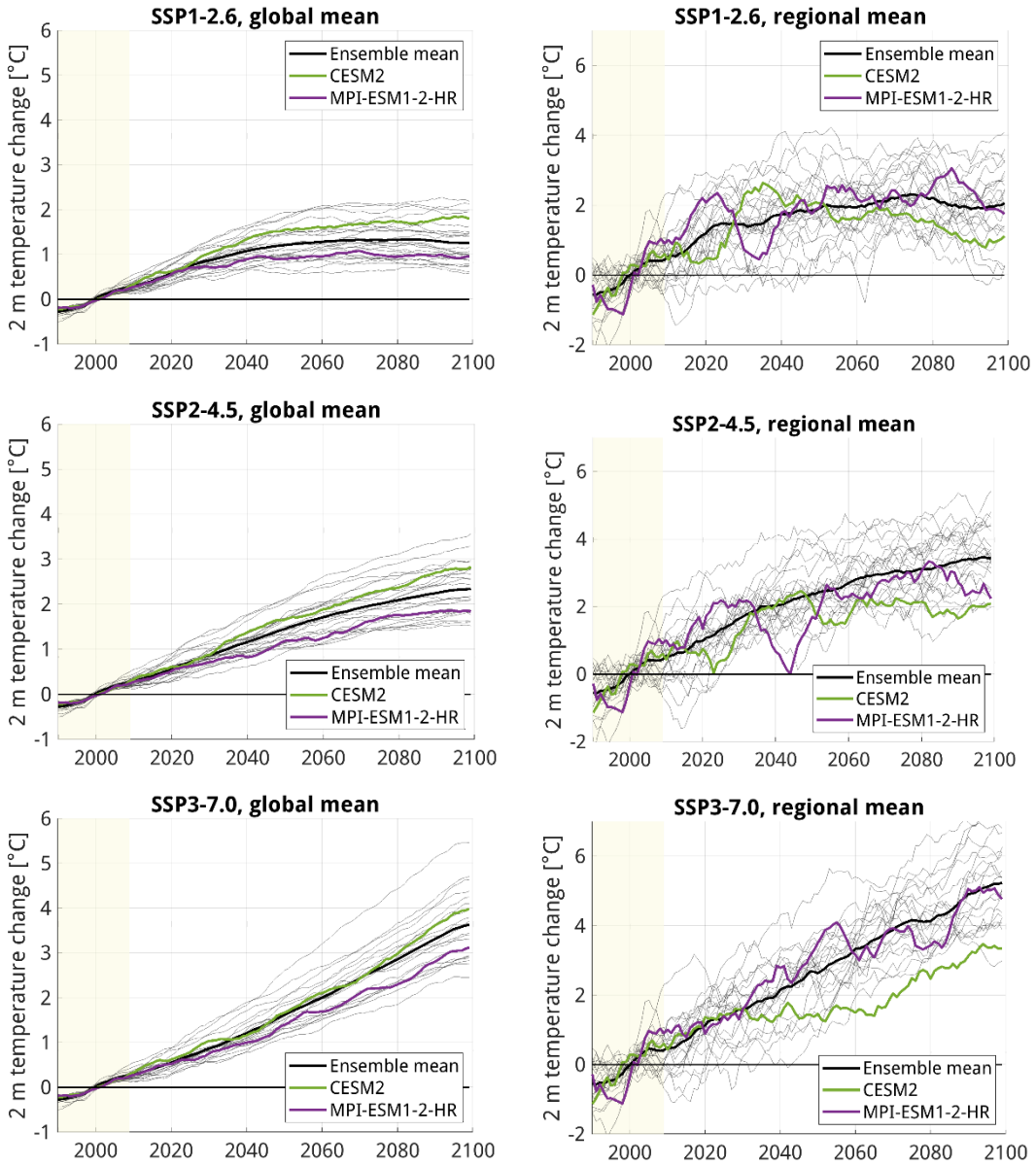

Figure 1: Global (top) and regional (bottom) mean evolution of 2 m temperature anomalies relative to the mean of 1990-2009 (yellow shaded area) for the ensemble mean (black line) and individual (grey and colored lines) CMIP6 models for three different SSP/RCP combinations. Each line shows 10-year moving averages for the winter season only (DJF). The regional means are approximately averaged over the WRF domain shown in Figure 2.

2.2 Regional model configuration and downscaling

WRF version 4.1.2 is used for dynamical downscaling of the GCM data. The model is set up with one domain with a horizontal resolution of 12 km (Fig. 2) and 32 vertical levels. No cumulus parameterization is used so convection is resolved explicitly. Model parameterization choices are listed in Table 1. The Thompson and Eidhammer microphysics scheme is chosen due to its explicit development and extensive testing for winter conditions [13,14], in addition to its successful use in simulating atmospheric icing conditions [15, 16, 17, 18, 19, 20]. A modification has been made to the microphysics scheme regarding the representation of melting snow, to ensure accurate predictions of wet snow icing, which is documented in [21].

Boundary conditions are updated in WRF every 6 hours and spectral nudging to the data from CESM2 and MPI-ESM1-2-HR is applied for temperature, horizontal winds and geopotential height. Sea-surface temperatures were also from the GCMs and updated daily in WRF.

The historical simulations are initialized on September 1, 1988, and the first 16 months are considered spin-up and not part of the analysis. The future simulations are initialized on January 1, 2015, restarting from the historical simulations. Other than changing the meteorological initial and boundary conditions and the greenhouse gas volume mixing ratios in the radiation schemes, no other changes, such as land cover changes, are made in the WRF simulations for the future time periods.

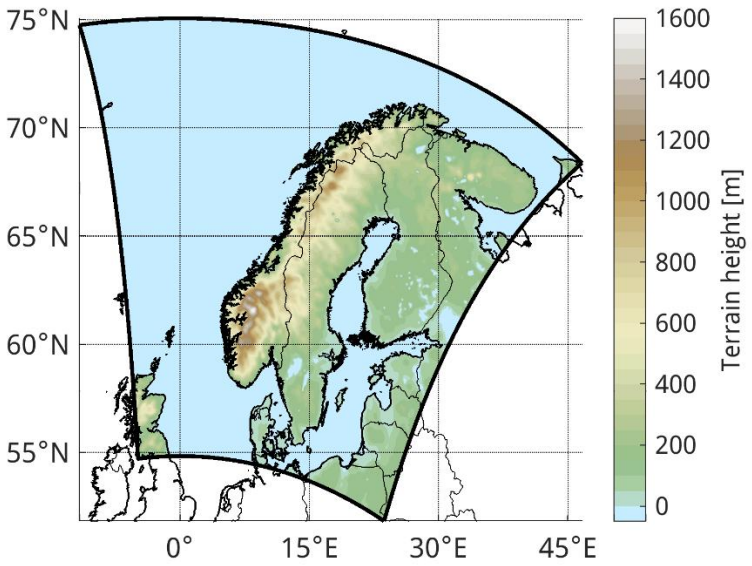

Figure 2: Spatial extent and terrain height of the 12 km x 12 km resolution WRF domain.

Table 1: Parameterization scheme choices for the WRF model configuration.

Type of scheme	**Name**
Microphysics	Thompson-Eidhammer aerosol-aware [14]
Boundary layer	MYNN2 [22]
Radiation	RRTMG [23]
Land surface	Noah [24]

2.3 Icing model

Hourly outputs from the WRF simulations are used to generate time series of both wet snow and rime ice accretion for each WRF grid point. Calculations of ice accretion are based on the model described in [25] which yields ice accretion rates on a reference collector[1]. The two icing types are calculated separately. Our icing models also include melting and sublimation processes, and other features developed through extensive research and testing (see below).

For rime ice, the key WRF output variables on which the icing calculations are based include temperature, wind speed, cloud water content and cloud droplet number concentration. For this icing type an adjustment to the accretion model regarding the cloud droplet size distribution has been made, based on research within the Icebox project [26].

For wet snow, the key WRF input variables to the model include temperature, air humidity, precipitation and wind speed. The temperature and air temperature are combined into one single variable, the wet-bulb temperature. This ice accretion model is also based on research by [17], with updates in several features from the ongoing Icebox project. The model now also allows for dry snow to accumulate, provided that the conductor is already covered with a layer of wet snow.

3. Results

In the following subchapters, data resulting from the downscaling of the global models, CESM2 and MPI, with the regional model WRF, and the icing calculations are presented. The datasets are hereafter referred to by WRF-CESM and WRF-MPI, and when relevant, with the associated SSP scenario. The analysis work is ongoing, and so preliminary results are presented.

3.1 Validation of historic climate

A validation of the simulated historic period (1990-2014) temperature and precipitation is performed with gridded observational data (E-OBS) [27]. As can be seen in Figure 3, both datasets are mostly colder than the observations over Norway, WRF-MPI more so than WRF-CESM. WRF-CESM displays a cold bias of about -0.5 – -2.5 ºC, but a small warm bias over East Norway (Fig. 3, top right panels), and WRF-MPI a bias of about -1.5 – -4 ºC. WRF-CESM temperature validates relatively well for winter, spring and fall (Fig. 3, top left), when atmospheric icing mainly occurs. WRF-MPI is too cold throughout the year. For precipitation, both models are mostly too wet compared to the observations, WRF-CESM more so than WRF-MPI (Fig. 3, bottom right panels). WRF-CESM show a wet bias of 1 – 150%, with the largest bias occurring over elevated areas. WRF-MPI show mostly a wet bias of about 1 – 100%, where the largest bias occurs over the northernmost part of the map. The wet bias over other elevated areas is restricted to about 75%. There is a relatively small (0 – 40%) dry bias along the coastline. For the icing seasons, it is clear that WRF-MPI validates best for precipitation (Fig. 3, bottom left). It should be noted that the E-OBS data is particularly uncertain in elevated areas during winter months, due to challenges in measuring precipitation as snow in typically high wind conditions.

[1] Rotating, vertical cylinder (length = 1 m, diameter = 0.03 m)

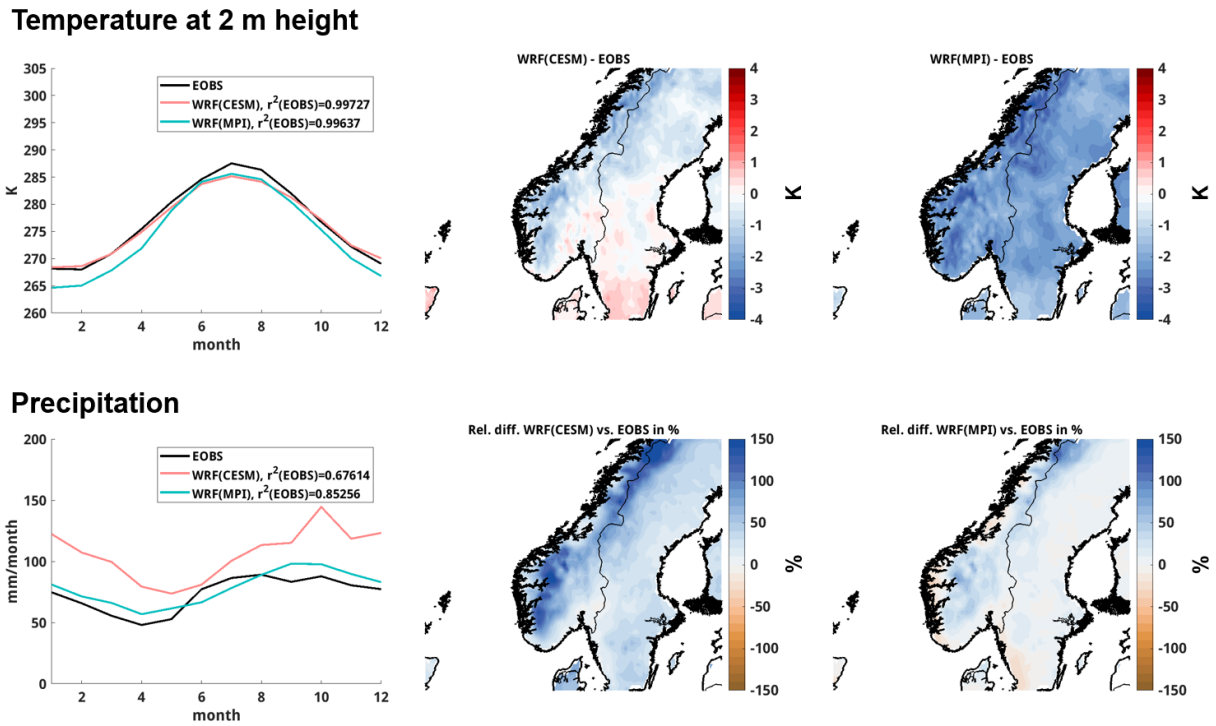

Figure 3: Comparisons of the WRF-CESM and WRF-MPI historical periods (1990-2014) with gridded observations (E-OBS) of temperature (2 m) and precipitation [28]. The graphs in the left panels are averaged over the spatial region (land only) shown in the maps.

3.2 Future changes

3.2.1 Wet snow

Figure 4 shows the change in mean wet-bulb temperature (the "wet" temperature, which is used in the wet snow icing model) (left) and winter precipitation total (right) between the historic and future 30-year periods, 1990-2019 and 2070-2099, respectively. WRF-MPI shows a higher degree of warming than WRF-CESM2. This is due to the the North Atlantic warming hole (NAWH) being more prominent in CESM2 (as mentioned in section 2.1). For the ssp126 scenario, WRF-CESM2 is even cooling (less than 1 ºC) off the coast of west-central Norway. For both models, warming is increasing from west to east, also due to the cooling effect of the NAWH. Warming is also increasing with the severity of the future scenario.

The pattern of change in winter (Nov-March) precipitation is less consistent among the projections compared to temperature. WRF-CESM2 generally shows a precipitation decrease over large parts of western and northern Norway (down to -30%), and an increase along the westernmost and southern coastline, and over eastern Norway (up to about 20%). For ssp245 this pattern is less prominent and there is a relatively small (less than 5%) increase over south-western Norway and Nordland County. For WRF-MPI ssp126 there is a west-east divide in the signal sign. For ssp 245 there is no clear signal, and for ssp370 there is a precipitation decrease over all of Norway.

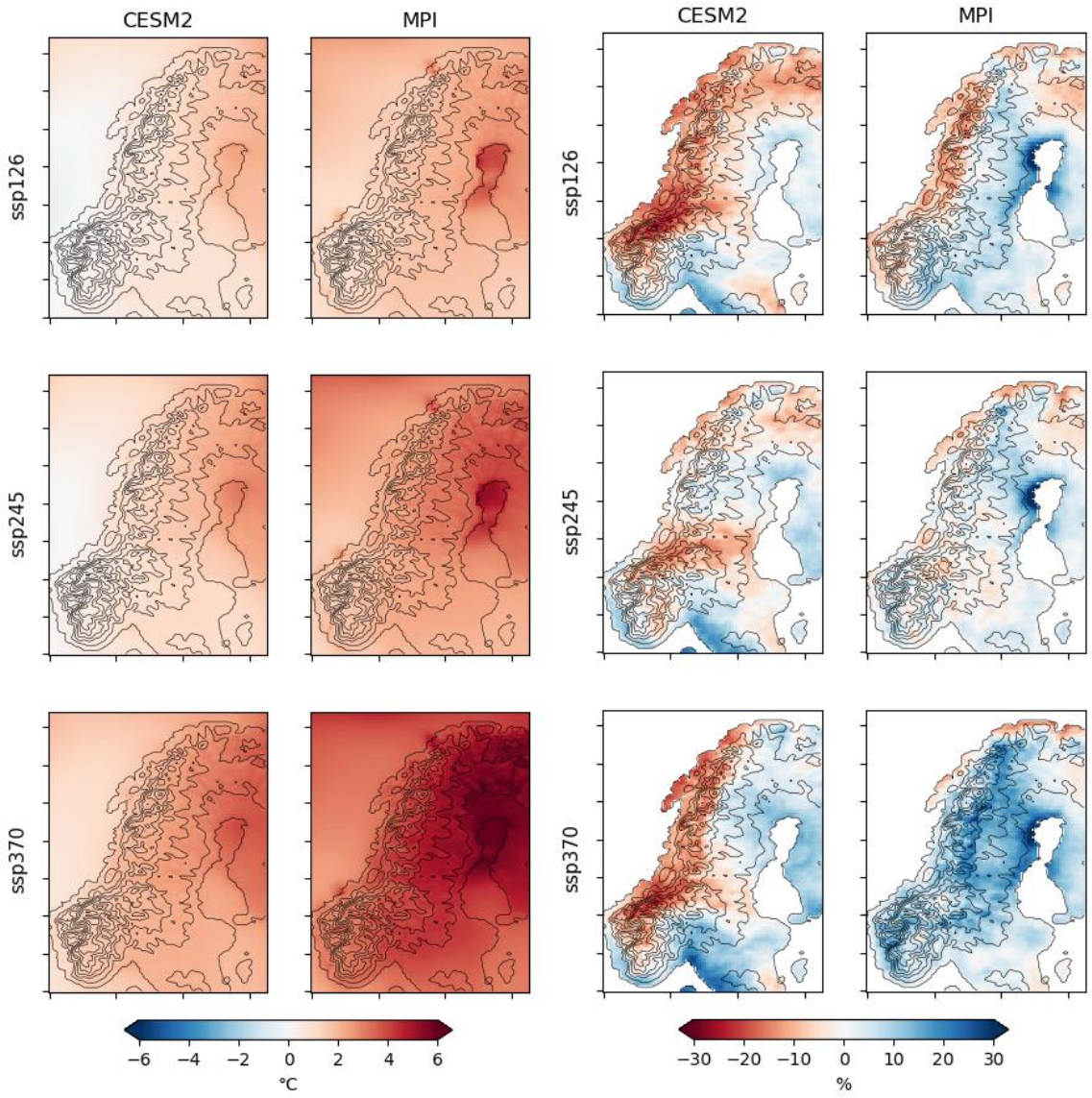

Figure 4: Change in winter (Nov-March) mean wet-bulb temperature (ºC) (left) and winter precipitation total (%) (right) between the future period 2070-2099 and the historic period 1990-2019, for the models WRF-CESM2 and WRF-MPI and the scenarios ssp126, ssp245 and spp370.

Figure 5 shows the change in total annual wet snow load. It seems like this pattern of change to a large extent is influenced by the change in precipitation. In WRF-CESM2 ssp126 and ssp245 there is increased wet snow total along the westernmost coastline, consistent with the precipitation increase. In the most elevated western mountains, wet snow is decreasing, consistent with the precipitation decrease. Though, for WRF-CESM2 ssp370, there is a tendency towards a decrease along the same stretch of coastline (also evident for a few of the lowest lying grid points in ssp245), indicating that the precipitation will fall as rain more often in these low-lying areas. In areas experiencing increased wet snow, but decreased precipitation, temperature is the most influential parameter, shifting the local climate in favour of wet snow. WRF-MPI shows a general pattern of increased wet snow total above about 400 m.a.s.l., where the precipitation effect dominates, and decrease below, where the temperature effect dominates.

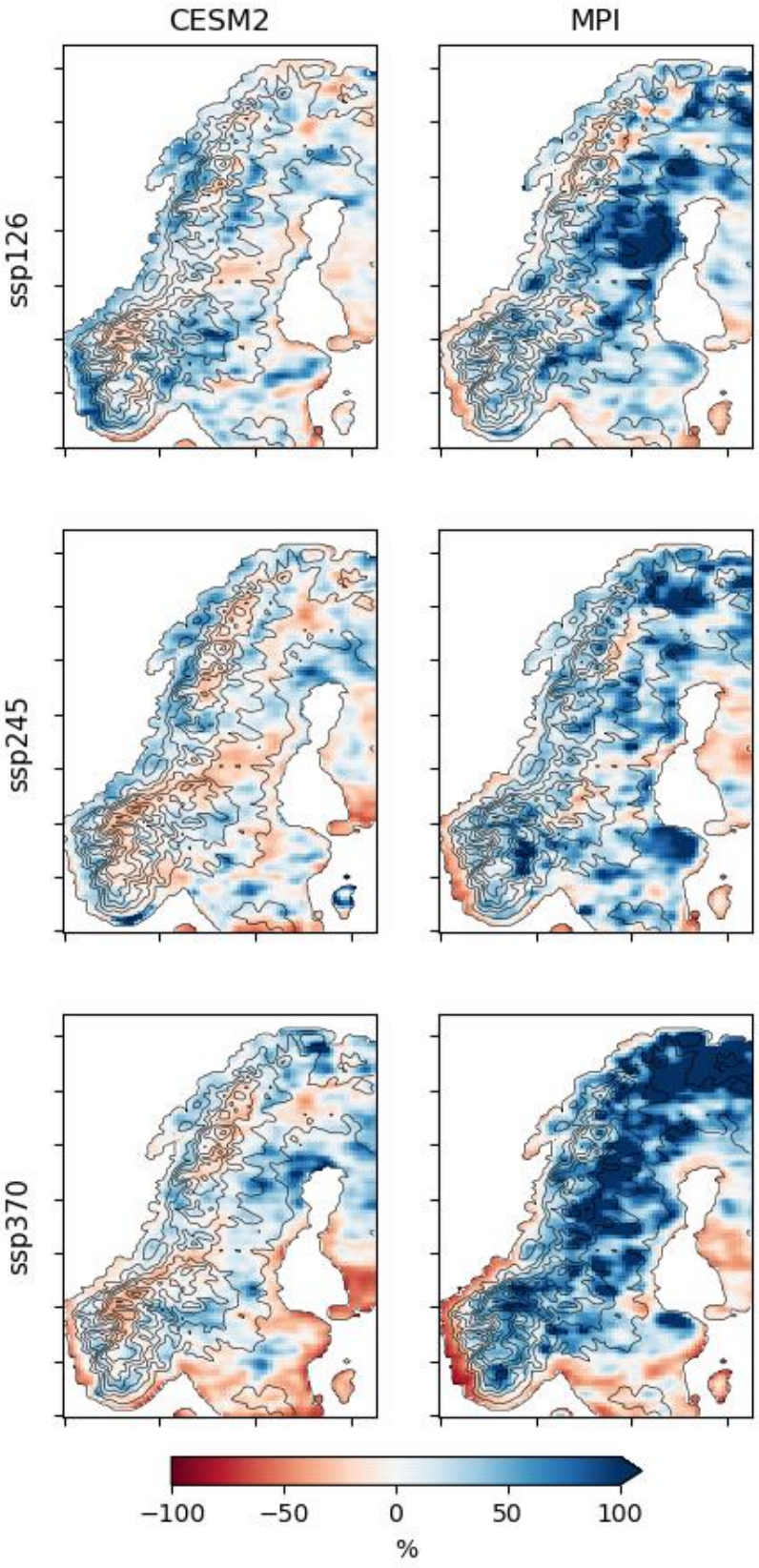

Figure 5: Change in total annual wet snow load (%) between the future period 2070-2099 and the historic period 1990-2019, for the models WRF-CESM2 and WRF-MPI and the scenarios ssp126, ssp245 and spp370.

3.2.2 Rime ice

For rime ice, temperature and cloud water are the most influential variables. The signal for (dry) temperature (Fig. 6, left-) is similar to that of the wet temperature (Fig. 4, left). For cloud water there seems to be a consensus between the models of a general increase over elevated terrain and a decrease in the low land (Fig. 6, right). WRF-CESM2 also shows increased cloud water along the west coast, and a tendency of a decrease in the north-western mountains (coinciding to some extent with the area of precipitation decrease (Fig. 4, right)).

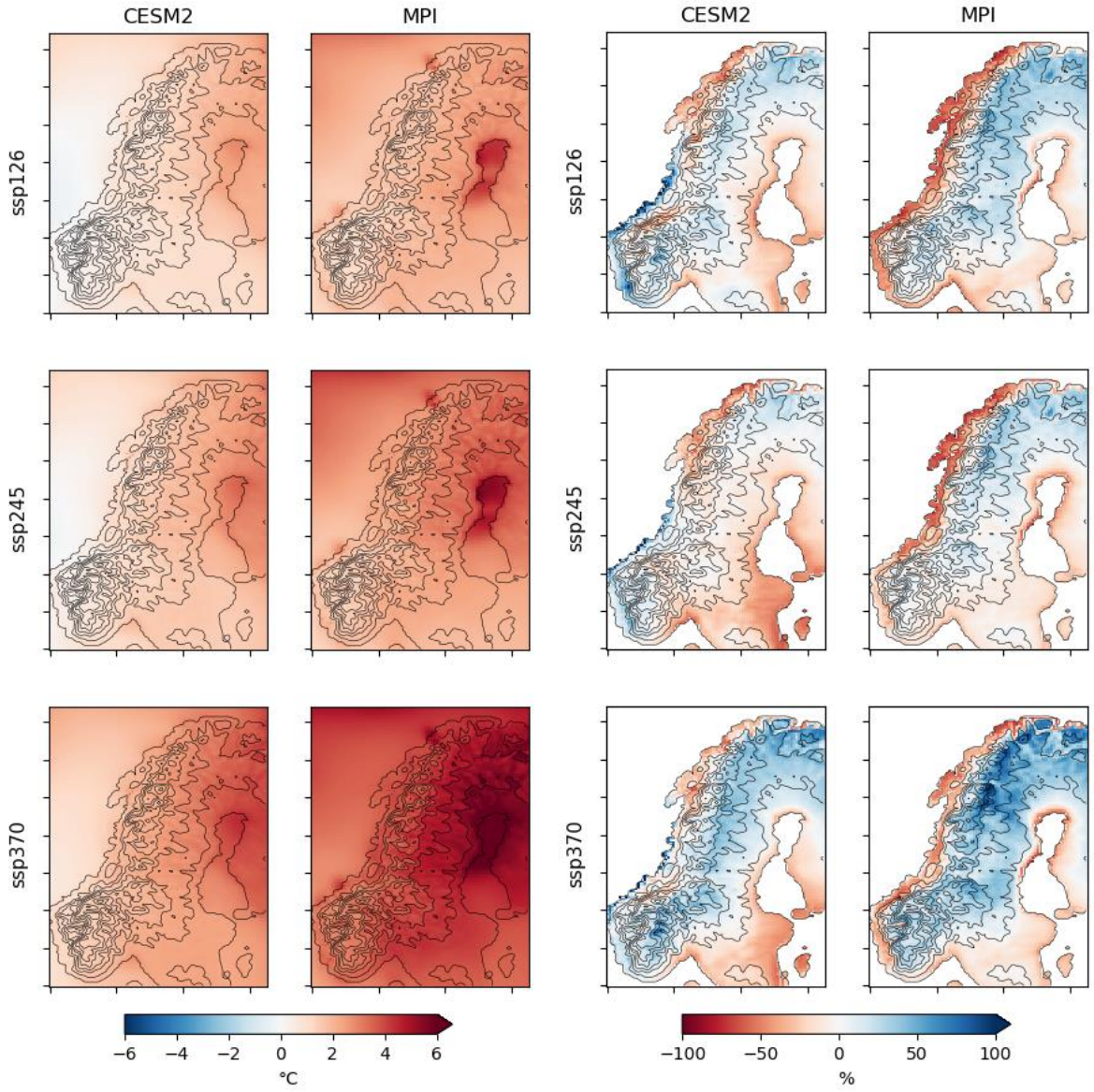

Figure 6: Change in winter (Nov-March) mean temperature (ºC) (left) and winter cloud water total (%) (right) between the future period 2070-2099 and the historic period 1990-2019, for the models WRF-CESM2 and WRF-MPI and the scenarios ssp126, ssp245 and spp370.

Figure 7 shows the change in maximum rime ice load (kg/m) between the historic and future periods. This does not give insight into the change in icing frequency but indicates the maximum loads that are able to accumulate, which is decisive for the OHL designers. There is disagreement between the models, where WRF-CESM2 projects mostly increased maximum ice loads and WRF-MPI reductions in many areas, particularly northern Norway. The signal is not as clear over the southern half of the country in WRF-MPI, but there might be a signal of increased maximum ice loads along the most

elevated west-facing mountain slope (not evident for ssp370 where increased temperature might be dominating the signal). Even though there generally is a larger increase in cloud water over land in WRF-MPI, the associated stronger warming seems to dominate the signal in maximum rime ice loads. Warmer temperatures imply more frequent melting episodes, shorter periods of ice accumulation, and hence smaller ice loads.

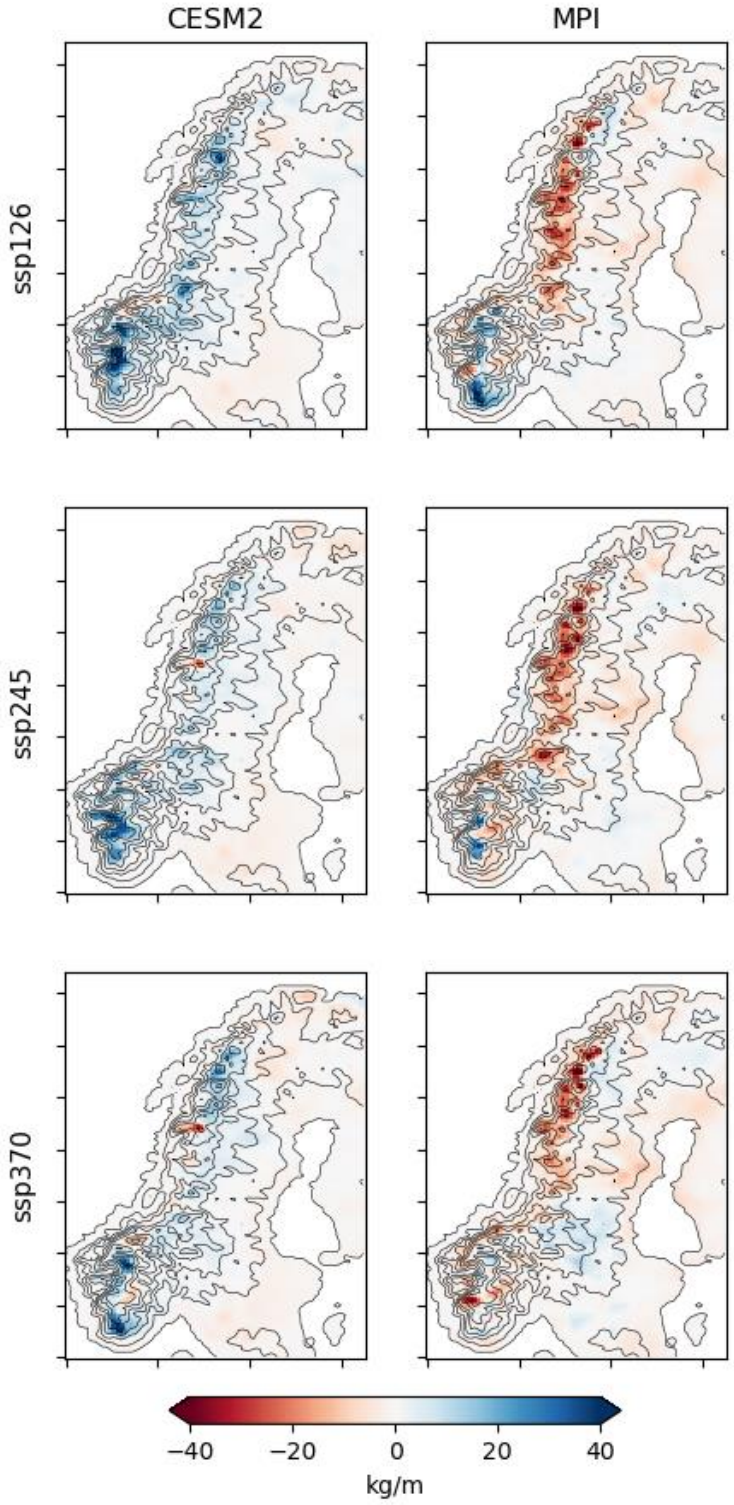

Figure 7: Change in period maximum rime ice load (kg/m) between the future period 2070-2099 and the historic period 1990-2019, for the models WRF-CESM2 and WRF-MPI and the scenarios ssp126, ssp245 and spp370.

4. Summary and further work

The downscaled climate data generally shows an increase in temperature everywhere, except for a relatively small cooling over the North Sea in WRF-CESM2 for the less extreme scenarios. This, and the general increase in warming from west to east is due to the North Atlantic Warming hole, which is more prominent in CESM2. The signal in precipitation is less clear, and there are large differences between the two models. For the most extreme scenario (ssp370) where the signals are most prominent, WRF-CESM2 shows decreased precipitation over most of Norway (except southernmost and eastern) while WRF-MPI shows an increase over all of Norway. There is stronger agreement in the cloud water signal, where there is a general increase over elevated terrain and decrease in the low land.

Preliminary results of the wet snow icing calculations indicate that change in annual wet snow load total will follow the pattern of precipitation to a large extent, however for coastal, low altitude areas the increased temperature seems to have the largest impact on the total wet snow loads in terms of a reduction. Given that the signal in precipitation is so different between the models, as described, the signal in wet snow load is also varying. Generally wet snow totals are decreasing for terrain below about 400 m.a.s.l. and increasing above, though not true everywhere for WRF-CESM2 which shows cooling to the west and drying in western mountains.

The signal in maximum rime ice load is also very different between the models, where WRF-CESM2 projects a general increase and WRF-MPI a general decrease. This is probably mostly connected to the stronger warming in WRF-MPI, which creates more melting episodes.

4.1 Further work

Further analysis will investigate signal-to-noise ratios and statistical significance of the climate change signals in icing.

As we now possess continuous timeseries of atmospheric ice loads from 1990 to 2099, we can also perform extreme value analyses to estimate ice loads with specified return period for different time horizons. We aim at calculating 50-year return period ice loads for 30-year time chunks, where the historic period constitutes 1990 – 2019.

Given a historic 30-year period and three future 30-year periods with estimated 50-year return period ice loads, we are able to investigate the future change. Given the total of six model simulations (two climate models and three scenarios) we will possess a span in the estimated 50-year return period ice loads, where the spread can be used as a basis for estimation of uncertainty. This will be used to create maps of the change in 50-year return period loads for rime ice and wet snow for the three future periods. The level of uncertainty can for example be added as a new layer to the map.

BIBLIOGRAPHY

[1] Nygaard, B.E.K. and S. M. Fikke. “Isstorm, Ising på kraftforsyningsnettet”. (Norges vassdrags- og energidirektorat – rapport 44, 2012).

[2] Ranasinghe, R., A. C. Ruane, R. Vautard, N. Arnell, E. Coppola, F. A. Cruz, S. Dessai, A. S. Islam, M. 6 Rahimi, D. Ruiz Carrascal, J. Sillmann, M. B. Sylla, C. Tebaldi, W. Wang, R. Zaaboul. “Climate Change Information for Regional Impact and for Risk Assessment”. (In: Climate Change 2021: The Physical Science Basis. Contribution of Working Group I to the Sixth Assessment Report of the Intergovernmental Panel on Climate Change [Masson-Delmotte, V., P. Zhai, A. Pirani, S. L. Connors, C. Péan, S. Berger, N. Caud, Y. Chen, L. Goldfarb, M. I. Gomis, M. Huang, K. Leitzell, E. Lonnoy, J. B. R. Matthews, T. K. Maycock, T. Waterfield, O. Yelekçi, R. Yu and B. Zhou (eds.)]. Cambridge University Press, 2021. In Press).

[3] Skamarock, W. C., Klemp, J. B., Dudhia, J., Gill, D. O., Liu, Z., Berner, J., . . . Huang, X.-Y. “A Description of the Advanced Research WRF Version 4”. (NCAR/TN-556+STR: NCAR Tech. Note, 2019).

[4] Hurrell, J. W., Kushnir, Y., Ottersen, G., and Visbeck, M. “The North Atlantic Oscillation: Climatic Significance and Environmental Impact” (134 ed. Washington, DC: American Geophysical Union, 2003).

[5] Eyring, V., Bony, S., Meehl, G. A., Senior, C. A., Stevens, B., Stouffer, R. J., and Taylor, K. E. “Overview of the Coupled Model Intercomparison Project Phase 6 (CMIP6) experimental design and organization” (Geosci. Model Dev., 9, 1937–1958, 2016. https://doi.org/10.5194/gmd-9-1937-2016).

[6] O'Neill, B. C., Tebaldi, C., van Vuuren, D. P., Eyring, V., Friedlingstein, P., Hurtt, G., Knutti, R., Kriegler, E., Lamarque, J.-F., Lowe, J., Meehl, G. A., Moss, R., Riahi, K., and Sanderson, B. M. “The Scenario Model Intercomparison Project (ScenarioMIP) for CMIP6” (Geosci. Model Dev., 9, 3461–3482, 2016. https://doi.org/10.5194/gmd-9-3461-2016).

[7] Danabasoglu, G., Lamarque, J.-F., Bacmeister, J., Bailey, D. A., DuVivier, A. K., Edwards, J., et al. “The Community Earth System Model Version 2 (CESM2)”. (Journal of Advances in Modeling Earth Systems, 12, e2019MS001916, 2020. https://doi.org/10.1029/2019MS001916).

[8] Müller, W. A., Jungclaus, J. H., Mauritsen, T., Baehr, J., Bittner, M., Budich, R., et al. “A higher-resolution version of the Max Planck Institute Earth System Model (MPI-ESM1.2-HR)” (Journal of Advances in Modeling Earth Systems, 10, 1383– 1413, 2018. https://doi.org/10.1029/2017MS001217).

[9] Cai, Z., You, Q., Wu, F., Chen, H. W., Chen, D., and Cohen, J. “Arctic Warming Revealed by Multiple CMIP6 Models: Evaluation of Historical Simulations and Quantification of Future Projection Uncertainties” (Journal of Climate, 34(12), 4871-4892, 2021).

[10] Zelinka, M. D., Myers, T. A., McCoy, D. T., Po-Chedley, S., Caldwell, P. M., Ceppi, P., Klein, S. A., and Taylor, K. E. “Causes of higher climate sensitivity in CMIP6 models” (Geophys. Res. Lett., 47, e2019GL085782, 2020. https://doi.org/10.1029/2019GL085782).

[11] Keil, P., Mauritsen, T., Jungclaus, J. et al. “Multiple drivers of the North Atlantic warming hole” (Nat. Clim. Chang. 10, 667–671, 2020. https://doi.org/10.1038/s41558-020-0819-8).

[12] Meehl, G. A., Arblaster, J. M., Bates, S., Richter, J. H., Tebaldi, C., Gettelman, A., et al. “Characteristics of future warmer base states in CESM2” (Earth and Space Science, 7, e2020EA001296, 2020. https://doi.org/10.1029/2020EA001296).

[13] Thompson, G., P. R. Field, W. R. Hall, and R. M. Rasmussen. “Explicit forecasts of winter precipitation using an improved bulk microphysics scheme. Part II: Implementation of a new snow parameterization” (Mon. Wea. Rev., 136, 5095-5115, 2008).

[14] Thompson, G. and T. Eidhammer. “A study of aerosol impacts on clouds and precipitation development in a large winter cyclone” (J. Atmos. Sci., 71, 3636–3658, 2014).

[15] Thompson, G. R., B. E. Nygaard, L. Makkonen, and S. Dierer. “Using the weather research and forecasting (WRF) model to predict ground/structural icing” (In Proc. 13th Int. Workshop on Atmospheric Icing on Structures , pp 8., 2009).

[16] Nygaard, B. E. K., J. E. Kristjánsson, and L. Makkonen. “Prediction of in-cloud icing conditions at ground level using the WRF model” (J. Appl. Meteorol. Climatol., 50(12), 2445–2459, 2011. doi:10.1175/JAMCD-11-054.1).

[17] Nygaard, B.E.K., H. Ágústsson and K. Somfalvi-Tóth. “Modeling wet snow accretion on power lines: Improvements to previous methods using 50 years of observations” (J. Appl. Meteor. Climatol., 52(10), pp. 2189–2203, 2013).

[18] Elíasson, Á. J., S. P. Ísaksson, H. Ágústsson, and E. Thorsteins. “Wet-snow icing: Comparing simulated accretion with observational experience” (In Proc. 16th Int. Workshop on Atmospheric Icing of Structures (IWAIS), Uppsala, Sweden , pp. 9., 2015).

[19] Haldar, A. et al. “Rime Icing Model Validation Using WRF and Full Scale Field Icing Data” (CEATI report no. T113700-3384, Montreal, Canada, 2016).

[20] Nygaard, B.E.K., Ø. Byrkjedal, E. Iversen, M. Fredbo, H. Ágústsson, and Ø. “Welgaard Development of a reliable modeling system for the calculation of rime ice loads on overhead transmission lines” (In-Proc. IWAIS, 2017).

[21] Iversen, E. C., Thompson, G., and Nygaard, B. “Improvements to melting snow behavior in a bulk microphysics scheme” (J. Atmos. Res., 253, 105471, 2021. https://doi.org/10.1016/j.atmosres.2021.105471)

[22] Nakanishi, M., Niino, H. “An Improved Mellor–Yamada Level-3 Model: Its Numerical Stability and Application to a Regional Prediction of Advection Fog” (Boundary-Layer Meteorol., 119(2), pp. 397-407, 2006).

[23] Iacono, M. J., Delamere, J. S., Mlawer, E. J., Shephard, M. W., Clough, S. A., Collins, W. D. “Radiative forcing by long-lived greenhouse gases: Calculations with the AER radiative transfer models” (J. Geophys. Res., 113(D13103), 2008).

[24] Mitchell, K. “NCAR: Unified Noah LSM” (https://ral.ucar.edu/sites/default/files/public/product-tool/unified-noah-lsm/Noah_LSM_USERGUIDE_2.7.1.pdf [accessed 12 February 2020], 2005).

[25] Makkonen, L. “Models for the growth of rime, glaze, icicles and wet snow on structures” (Phil. Trans. R. Soc. A. 3582913–2939, 2000. http://doi.org/10.1098/rsta.2000.0690).

[26] Sokolov, P. and Virk, M.S. “Droplet Distribution Spectrum Effects on Dry Ice Growth on Cylinders” (Cold Regions Science and Technology, 160, 80 – 85, 2019. https://doi.org/10.1016/j.coldregions.2019.01.002).

[27] Cornes, R., G. van der Schrier, E.J.M. van den Besselaar, and P.D. Jones. “An Ensemble Version of the E-OBS Temperature and Precipitation Datasets” (J. Geophys. Res. Atmos., 123, 2018. doi:10.1029/2017JD028200).